Metal-free, visible light-mediated atom transfer radical polymerization of hydroxypropyl cellulose-graft-poly(methyl methacrylate)s: effect of polymer side chains on thermo-responsive behavior of hydroxypropyl cellulose

Muhammad Asif Iqbal · Toheed Akhter · Muhammad Faheem · Asif Mahmood · Waheed Al-Masry · Sohail Nadeem · Sadaf Ul Hassan · Chan Ho Park

Abstract We exploited organic photo-redox-catalyzed atom transfer radical polymerization (O-ATRP) to synthesize a thermo-responsive polymer with a narrow molecular weight distribution. Poly(methyl methacrylate) (PMMA) chains were polymerized from a hydroxypropyl cellulose (HPC)-based macroinitiator using metal-free O-ATRP under visible-light irradiation. This O-ATRP is mediated by 1,2,3,5-tetrakis (carbazol-9-yl)-4,6-dicyanobenzene (4CzIPN), a photoredox catalyst with a substantial excited-state reduction potential, low cost, and ease of preparation. The synthesis of a series of PMMA-grafted HPC (PMMA-*g*-HPC) was characterized by various analytical methods, including FTIR spectroscopy, NMR spectroscopy, TGA, and GPC analysis. The lower critical solution temperature (LCST) of the polymers was determined by measuring the transmittance of the polymer solution as a function of the temperature at various pH values. Consequently, we expanded the LCST window of the HPC-based polymers and generated the opposite pH dependency of the LCST by forming PMMA-*g*-HPCs. Our "grafting-from" synthetic approach and thermo-responsive polymers, which are controllable in full range of physiological conditions, are promising in a variety of biological, electronics, and biosensor applications, particularly in drug delivery systems.

M. A. Iqbal · T. Akhter (✉) · M. Faheem · S. Nadeem
Department of Chemistry, School of Science,
University of Management and Technology, C-II,
Johar Town, Lahore 54770, Pakistan
e-mail: Toheed.akhter@umt.edu.pk

A. Mahmood · W. Al-Masry
Department of Chemical Engineering, College
of Engineering, King Saud University, Riyadh 11421,
Saudi Arabia

S. U. Hassan
Department of Chemistry, COMSATS University
Islamabad, Lahore Campus, Lahore, Pakistan

C. H. Park (✉)
Department of Chemical and Biological Engineering,
Gachon University, 1342 Seongnam-daero,
Seongnam 13120, Republic of Korea
e-mail: chhopark@gachon.ac.kr

Introduction

Smart polymer-based systems capable of experiencing modifications in response to various stimuli are of particular interest (Cobo et al. 2015; Jia et al. 2022). Smart polymers/stimuli-responsive polymers are at the forefront of various technologies because they show an active response to every small stimulus, resulting in large alterations in their

microstructure, as well as physiological and chemical properties (Park et al. 2018). Smart polymers can be graft copolymers, homopolymers, or block copolymers, depending on their topology (Sikdar et al. 2021). The graft modification of stimulus-responsive materials is appealing for the fabrication of smart polymers (Jana and Uchman 2020; Kang et al. 2013). Different biomacromolecules, including dextran, keratin, cellulose and its derivatives, have been used as the backbones for the synthesis of this type of smart polymers (Cobo et al. 2015; Garcia-Valdez et al. 2018). Cellulose and its derivatives are the most abundant polysaccharides and are mostly used as important sustainable raw materials (Yuan et al. 2012). Furthermore, cellulose has several appealing features including renewability, biocompatibility, and abundant availability in nature (Droguet et al. 2022). Hydroxypropyl cellulose (HPC), an important derivative of cellulose, is non-toxic, water-soluble, and has significant thermo-responsive properties, making it an attractive candidate for various biological applications (Arredondo et al. 2020; Barty-King et al. 2021; Hatton et al. 2017). The barrier of the lower critical solution temperature (LCST) of 40–45 °C, which falls outside the range of the physiological temperature (25–38 °C), hinders HPC from functioning as an important biomaterial (Rwei and Nguyen 2015). The LCST of HPC has been attempted to be regulated to the physiological temperature range or even to the body temperature via graft modification of HPC (Kedzior et al. 2019; Weißenborn and Braunschweig 2019). Many synthetic thermoresponsive polymers have been identified and extensively studied, including poly(methyl methacrylate)-*b*-poly(N-isopropyl acrylamide) (PMMA-*b*-PNIPAM) (Ko et al. 2020), oligo(ethylene glycol) methyl ether methacrylate (OEGMA) and poly(ethylene glycol) (Porsch et al. 2011), poly(methyl methacrylate)-*b*-P(NIPAAm-*co*-Nacryloxysuccinimide) (PMMA-*b*-P(NIPAAm-*co*-NAS) block copolymer (Chang et al. 2011), hydroxypropyl cellulose acrylic acid (HPC-AA) (Bai et al. 2012), and hydroxypropyl cellulose-*g*-poly(4-vinylpyridine) (HPC-*g*-P4VP) (Ma et al. 2010).

Poly(methyl methacrylate) is one of the most investigated polymers because of its stability, low cost, low optical loss in the visible spectrum, and ability to sense chemicals, which was also studied by employing its optical, electrical, and microgravimetric properties. Poly(methyl methacrylate) (PMMA) is a promising thermoresponsive polymer for use in sensors, analytical separation, pneumatic actuators, and optical and conductive devices. They can also be used for biomedical purposes, polymer electrolytes, and drug delivery systems (Saad et al. 2020).

The grafting of various synthetic thermoresponsive polymers on a cellulose backbone using several conventional techniques has been investigated comprehensively (Wohlhauser et al. 2018; Zhang et al. 2017). These techniques include reversible deactivation radical polymerization (RDRP), ring-opening polymerization, free radical polymerization, nitroxide-mediated polymerization (NMP), reversible addition-fragmentation chain transfer (RAFT) polymerization, atom transfer radical polymerization (ATRP), (Chen et al. 2016; Parkatzidis et al. 2020), and surface initiated ATRP (SI-ATRP), (Huang et al. 2015; Lacerda et al. 2013; Morandi et al. 2009; Tu et al. 2019; Yi et al. 2008). The majority of the employed techniques are based on free-radical polymerization processes, in which free-radical sites are synthesized along the cellulose backbone through chemical or irradiation means (Chen et al. 2016). The polymer chain grows from these radical sites using a "grafting-from" technique in the presence of vinyl monomers. Among these techniques, ATRP has been extensively used for controllable graft copolymerization of various vinyl monomers onto the cellulose backbone and derivatives of cellulose (Larsson et al. 2015). ATRP has become one of the most powerful techniques for precision polymer synthesis for a variety of industrial applications, such as cosmetics, detergents, paints, surfactants, coatings, adhesives, inkjet printing, and drug delivery systems (Kaldéus et al. 2019; Matyjaszewski 2018).

ATRP has traditionally depended on transition-metal-based catalysts to mediate its mechanism, which affords a polymer with a controlled molecular weight (MW), low Dispersity index (Đ), and controlled end-group functionality. However, transition metal contaminants remain permanently in synthesized polymeric products, limiting their applications in electronics and biomedical fields (Treat et al. 2014). To reduce these transition metal residues in the final polymers, purification is required, which can increase the cost of the process. The elimination of these transition metals is required for suitable

microelectronics and biomedical applications (Matyjaszewski and Tsarevsky 2014).

To address the major issues associated with conventional ATRP, organic photoredox-catalyzed atom transfer radical polymerization (O-ATRP) under visible light irradiation has been developed for the synthesis of metal-free polymers, gradually replacing conventional ATRP-based transition metal catalysts (de Ávila Gonçalves et al. 2021; Discekici et al. 2017; Miyake and Theriot 2014). Numerous investigations have been conducted on the O-ATRP employing organic photoredox catalysts. Matyjaszewski et al. first showed that phenyl phenothiazine analogs are very effective organic photoredox catalysts (OPCs) for the O-ATRP of methyl methacrylate (MMA) (Pan et al. 2016). Miyake et al. also developed various organic photoredox catalysts (perylene and diaryl dihydrophenazines) for O-ATRP (Theriot et al. 2016). Similarly, in our previous study, we reported further advancements in O-ATRP by formulating a design principle for the development of various organic photoredox catalysts (Singh et al. 2018).

In this study, we developed a metal-free O-ATRP for PMMA-grafted HPC (PMMA-*g*-HPC) with low Ð. O-ATRP using the HPC-based macroinitiator was carried out in the presence of 4CzIPN photoredox catalyst under visible-light irradiation. To assess the thermo-responsivity of the synthesized polymers, the LCST was determined by measuring the transmittance of the polymer solution as a function of temperature at different pH values. Grafting PMMAs onto HPC induced significant changes in the LCST and pH dependency. By tuning the MW of the grafted PMMA, the thermo-responsivity of PMMA-*g*-HPC was controlled over a full range of physiological conditions. To the best of our knowledge, O-ATRP has not been previously employed for the synthesis of such polymers, and the thermoresponsive behavior of PMMA-*g*-HPC has not been studied before.

Experimental

Materials

Hydroxypropyl cellulose (HPC) was purchased from carbosynth, UK (Mw = 180,456 gmol^{-1} according to manufacturer), 2-Bromopropionyl bromide (97%) was purchased from Alfa Aesar and used as received.

Methyl methacrylate (MMA, 99.0%) was purchased from Daejung, Dimethyl formamide (DMF, 99.8%) from RCI Labscan, Thailand, Dichloromethane (DCM, 99%) were purchased from Sigma Aldrich and used as received. 1,2,3,5-tetrakis(carbazol-9-yl)-4,6-dicyanobenzene (4CzIPN) was prepared using a reported method (Singh et al. 2018).

Synthesis of macroinitiators

The macroinitiator (HPC-Br) is prepared according to a reported procedure (Rahimian et al. 2015), as shown in Scheme 1a. HPC (2.456 g) was dissolved in 280 mL of anhydrous dichloromethane in a round bottom flask with continuous stirring overnight. Then, the solution was cooled to 0–5 °C in an ice bath and 2-Bromopropionyl bromide (186 mg, 0.8 mmol) solution in dichloromethane (40 mL) was added dropwise over 20 min. The reaction mixture was then stirred at room temperature (25 °C) for 24 h. Then, 20 mL of distilled water was added to the flask, and the mixture was allowed to stand until a sticky white solid material was obtained, which was filtered and dried under vacuum.

Synthesis of thermoresponsive polymers (PMMA-g-HPC)

Three different thermoresponsive polymers, denoted CP-06, CP-08, and CP-12, are synthesized via visible-light-driven O-ATRP in the presence of an organic photoredox catalyst, as shown in Scheme 1a. All these polymers differed in the molar ratios of HPC and PMMA. For instance, 94:06 (HPC: MMA), 92:08 (HPC: MMA), and 88:12 (HPC: MMA) were the molar ratios used to prepare CP-06, CP-08, and CP-12, respectively, based on the feeding ratio of monomer/macroinitiator for the reaction. Moreover, all these polymers were prepared using the same method, and the synthesis of CP-12 is discussed here as an example. The macroinitiator (225 mg) and anhydrous DMF (2 mL) were placed in a dried glass vial equipped with a stirring bar and a nitrogen inlet/outlet. After complete dissolution of the macroinitiator in DMF, MMA (1 mL) and 4CzIPN as an organic photoredox catalyst (10 mg) were added to the reaction mixture. Subsequently, the reaction mixture was bubbled with N$_2$ for 30 min. Further, polymerization was carried out for 6 h under blue light at room temperature in a closed system. The resulting polymer

product was precipitated in methanol (50 mL), filtered, and vacuum-dried separating residues including low molecular weight of free PMMA. The properties of the prepared polymers were compared with those of neat HPC, which is termed HPC-0 in this study.

Characterization and methods

FTIR spectra were recorded on a Bruker-Equinox 55 FTIR spectrometer using KBr pellets in the range $4000–400$ cm^{-1}. Proton nuclear magnetic resonance spectra (^{1}H NMR) were recorded on a Bruker ARX 400 MHz spectrometer. The structures of the polymers were characterized using DMSO as a solvent. Gel permeation chromatography (GPC) analysis was used to determine the molecular weight and Đ of the synthesized polymers using a 1200-inch series precision pump, 1200-inch series diode array detector and 1250-inch evaporative light scattering detector. The system was calibrated using polymethyl methacrylate (PMMA) standards. Thermogravimetric analysis (TGA) was performed using a Mettler Toledo 822 instrument. The LCST of the PMMA-g-HPC samples was measured using transmittance method. The thermoresponsive behavior of all polymers (HPC-0, CP-06, CP-08, and CP-12) was assessed by measuring the transmittance of the aqueous solutions (20 mg/mL) at a wavelength of 550 nm using a UV/Vis spectrophotometer (Shimadzu UV-2401PC), and the transmittance of the copolymer solutions as a function of temperature and pH was investigated in the temperature range of 20–70 °C. The pH of the aqueous solutions of all the polymers was adjusted by adding NaOH and HCl. The temperature at which 50% of the transmittance decreased was taken as the lower critical solution temperature (LCST). Similarly, the optical density (OD) of all the polymeric solutions (20 mg/mL) was measured at 550 nm by varying the temperature range from 20 to 70 °C at a heating rate of 5 °C/min using a UV/Visible spectrophotometer (Shimadzu UV-2401PC).

Results and discussion

Synthesis of macroinitiator

The synthesis of PMMA-g-HPC based thermoresponsive polymers is depicted in Scheme 1a. In this process, a macroinitiator (HPC-Br) was initially prepared by the reaction of HPC and 2-Bromopropionyl bromide. The structure of the prepared HPC-Br was evaluated using FTIR spectroscopy. The FTIR spectra of the monomer (HPC-O) and HPC-Br are shown in Fig. 1A. In case of HPC-0, the broad absorption band at 3460 cm^{-1} was attributed to the stretching vibrations of the hydroxyl group of cellulose. The absorption bands at 2993 and 2819 cm^{-1} were assigned to the C–H asymmetric and symmetric stretching vibrations of the methyl and methylene groups, respectively. As clear from FTIR spectrum of macroinitiator in the Fig. 1A (spectrum b), the absorption band at 1741 cm^{-1} was assigned to the stretching vibration of the carbonyl groups in the ester, and this absorption band is absent in the spectrum of HPC-0. The structure of the synthesized HPC-Br was also evaluated using NMR spectroscopy. In the ^{1}HNMR spectrum of the macroinitiator, a broad signal at 2.8 ppm (for one proton) is attributed to the proton of the methine group carrying the bromo group, shown as signal "c" in Fig. 1B. Furthermore, a resonance signal at 1.85 ppm (signal b) can be assigned to the methyl group of HPC backbone. Similarly, the methyl group of bromomethine resonated at 1.25 ppm (signal a). Moreover, by comparing the integral area of the signal for the methyl group of HPC backbone at about 1.25 ppm to that of the methyl proton of the 2-Bromopropionyl bromide group at around 1.85 ppm, the concentration of Br in term of degree of substitution was estimated to be 0.7, these results are in good agreement with previously published literature (Jin et al. 2013). In comparison, the NMR spectrum of HPC-0, reported elsewhere (Ci et al. 2017), does not have the peak "a" and "c" present at 1.25 ppm and 2.8 ppm in the NMR spectrum of macroinitiator.

Synthesis of PMMA-g-HPC polymers via O-ATRP

Three different thermoresponsive polymers (CP-06, CP-08, and CP-12) were prepared using MMA monomer and HPC-Br as macroinitiator via visible-light-mediated O-ATRP in the presence of 4CzIPN as a photoredox catalyst (Scheme 1a). Their synthesis has already been discussed above. The mechanism of O-ATRP is shown in Scheme 1b. O-ATRP is a versatile and efficient technique that harnesses the required energy from the visible light in the presence of a photoredox catalyst to initiate the controlled radical polymerization. In this mechanism, 4CzIPN
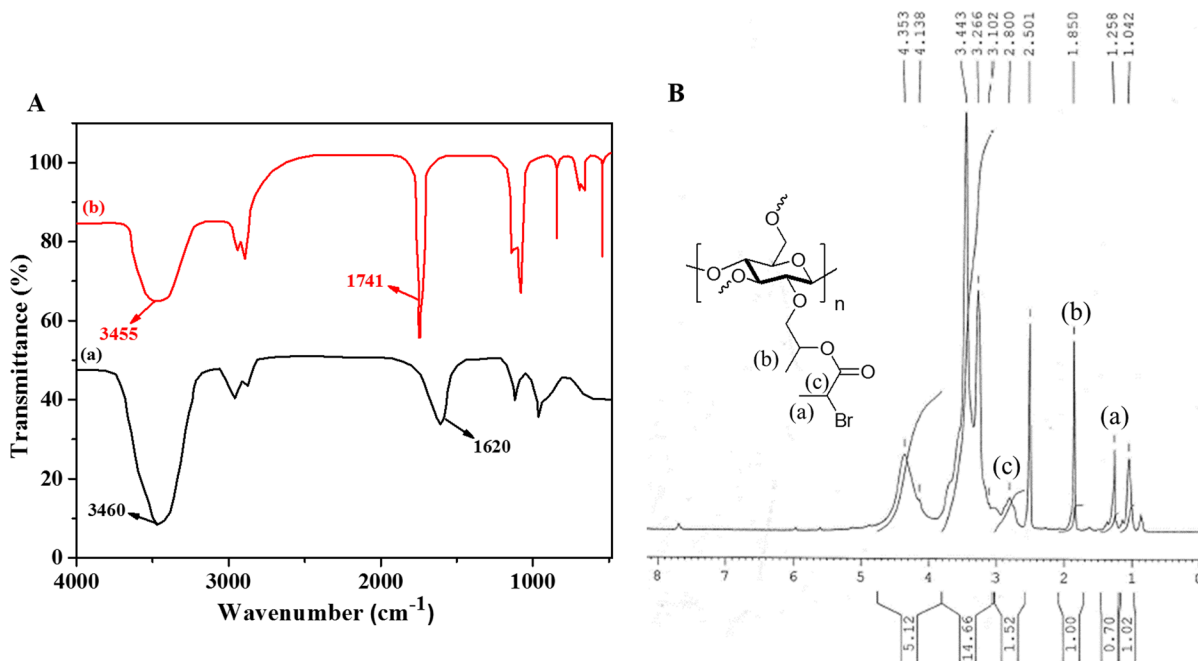
Fig. 1 **A** FTIR spectra of (a) HPC-0, (b) HPC-Br. **B** ^{1}H NMR spectrum of HPC-Br.

absorbs visible light in its ground state and is transferred to the excited state. This photoexcited species can reduce the macroinitiator by an oxidative process, leading to the formation of propagating radical (Pn.), bromide anion, and a radical cation. Afterwards, the polymer chains are propagated in a controlled way by the addition of the monomers. The deactivation process also runs side by side which can bring the propagating polymer chains to dormant phase, and the catalyst to the ground state, leading to the completion of the O-ATRP cycle. The mechanism of O-ATRP is well established and reported in a number of studies (Pan et al. 2016; Singh et al. 2018; Theriot et al. 2016).

The structures of PMMA-*g*-HPC polymers were evaluated by FTIR spectroscopy. As an example, the FTIR spectrum of CP-12 is given in the Fig. 2A where the absorption band of the carbonyl group was observed at 1734 cm^{-1} that was not observed in HPC-0 FTIR spectrum. It may indicate that the PMMA chains were successfully grafted onto the surface of hydroxypropyl cellulose. Similarly, the structures of the synthesized polymers were also confirmed using NMR spectroscopy, and ^{1}HNMR

spectra of CP-12 is given in the Fig. 2B as an example. In this ^{1}HNMR spectrum, the broad signal at 2.8 ppm disappeared which was present in the ^{1}HNMR spectrum of macroinitiator, which confirmed the conversion of the macroinitiator to the CP-12 polymer. Furthermore, the CP-12 polymer had a distinct chemical shift at 3.44 ppm that represents the three protons of OCH$_3$ of PMMA chains. Signals from HPC backbone of HPC grafted polymers are always very weak, in Fig. 2B the weak signals appearing below 2 ppm can be attributed to HPC backbone (Bagheri and Pourmirzaei 2013). While, the resonance peak above 7 ppm might be due to some unknown impurities. These results confirmed the successful grafting of PMMA chains onto the hydroxypropyl cellulose backbone.

GPC analysis

The molecular weight and Đ of HPC-0, CP-06, CP-08, and CP-12 were investigated by GPC analysis. The chromatograms of all polymers are shown in Fig. 2C, while the molecular weight and Đ values are given in Table 1. It is clear from the data that all the synthesized polymers have a narrow Đ,
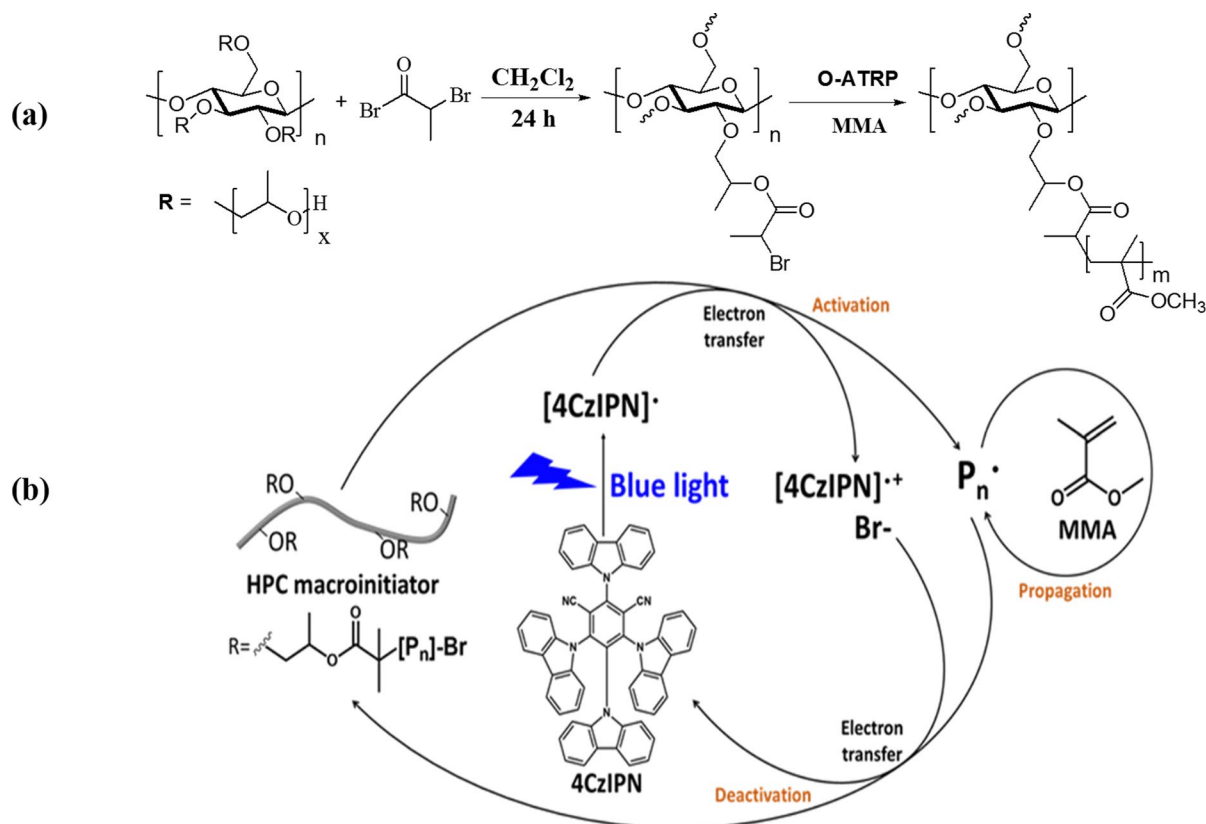
Scheme 1 **a** Synthesis of PMMA-*g*-HPC **b** Mechanism of the O-ATRP

1.2 in case of CP-06 while 1.1 in the case of CP-08 and CP-12, even at very high molecular weight values. Thus, it can be concluded that O-ATRP can be useful for preparing metal-contamination-free monodisperse polymers with a narrow Đ. Moreover, the hydrodynamic volume (Vh) of HPC-0, CP-06, CP-08, and CP-12 was calculated by Mark-Houwink equation and are presented in Table 1 (Kasaai 2008).

It is clear from these values that PMMA-*g*-HPC polymers have higher hydrodynamic volume than HPC-0, and in case of PMMA-*g*-HPC this value increases with increase in molecular weight of the polymer.

The kinetics of MMA polymerization on cellulose was also investigated using GPC analysis, CP-12 was used for the kinetic studies. Figure 3a displays a semilogarithmic plot of MMA monomer conversion versus reaction time, whereas M_o and M_t are the initial concentration and the concentration of the monomer

at the specific time. A linear variation in $\ln([M]_o/[M]_t)$ was observed from the start of polymerization to about three hours of the reaction time, which exhibited the first order kinetics during this time period. Afterwards, a small curvature in the graph showed deviation from the linear behavior. This could be due to the polar solvent (DMF) employed or a decrease in radical concentration, which would result in a partial termination of living free radicals. Moreover, the apparent propagation rate constant (k_{app}) was determined to be 0.03 h^{-1} using following equation (Dupayage et al. 2011);

$$ln\left(\frac{[M]_o}{[M]_t}\right) = (k_{app} \times t) \tag{1}$$

A slight variation in molecular weight and molecular weight distribution of PMMA side chains is depicted in Fig. 3b which further confirmed the polymerization kinetics. For this purpose, the CP-12

Fig. 2 A FTIR spectrum of
CP-12 polymer. **B** ^{1}H NMR
spectrum of CP-12 polymer.
C GPC Chromatograms of
HPC-0, CP-06, CP-08 and
CP-12.
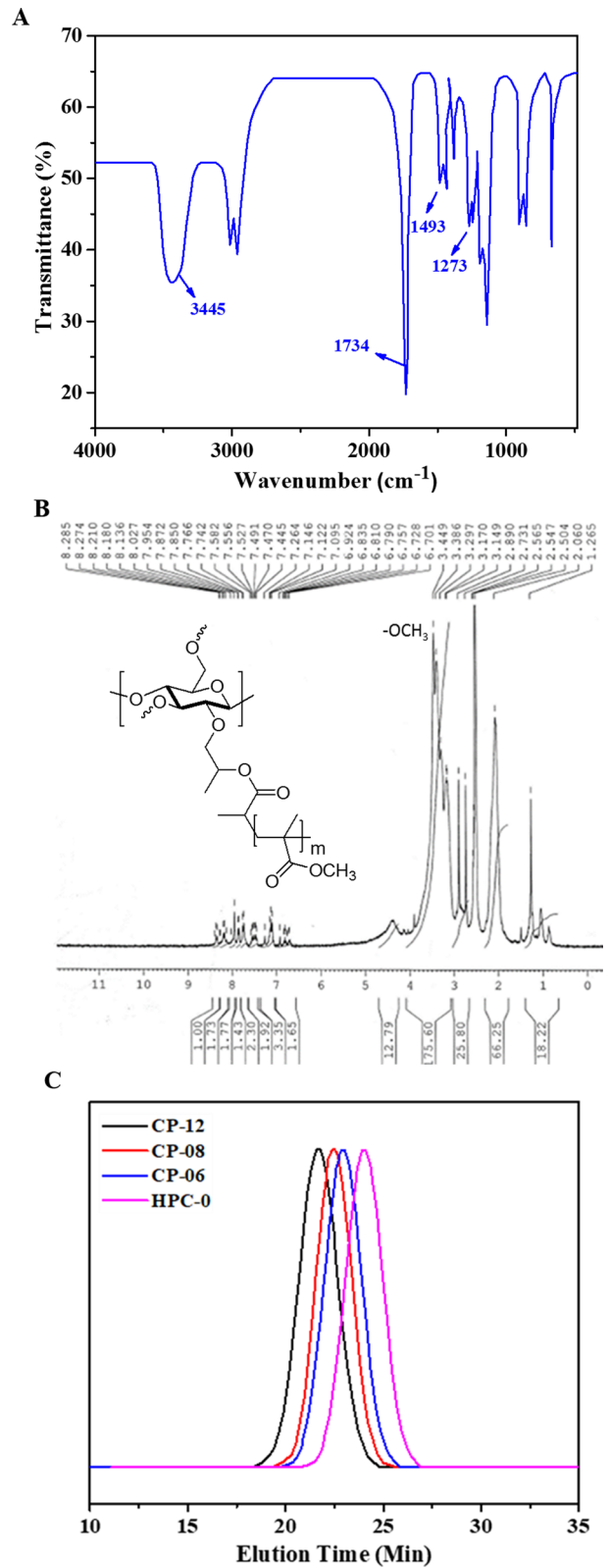
Table 1 M_n and Dispersity index (Đ), and hydrodynamic volume (Vh) of HPC-0, CP-06, CP-08 and CP-12.

Sample	M_n (g mol^{-1})	Đ	Vh (mL/mol)
HPC-0	180,456	1.8	1.61×10^6
CP-06	230,725	1.2	2.16×10^6
CP-08	252,620	1.1	2.40×10^6
CP-12	291,075	1.1	2.85×10^6

Reaction conditions: Synthesis of polymers was carried out in an inert atmosphere of nitrogen at 25 °C under the irradiation of 23 W, 455 nm blue LEDs (5 mW cm^{-2}). Molar of HPC: PMMA for each polymer is given in the Table, whereas 225 mg of macroinitiator were used in each case

M_n, Number average molecular weight; Đ, Dispersity index; Vh, Hydrodynamic volume

(Nada and Hassan 2000). TGA analyses of HPC-0, a macroinitiator, and synthesized polymers were carried out under an inert atmosphere of nitrogen. The thermal stabilities of macroinitiators HPC-0, CP-06, CP-08, and CP-12 were evaluated in terms of T_5, T_{10}, T_{50} and R_{600}, which are defined in Table 2. Figure 4 displays the thermograms of all samples. As is clear from the thermogram, HPC-0 was degraded in a single step with a value of $T_{50} = 375$ °C. In the case of the macroinitiator, the thermal stability was considerably decreased ($T_{50} = 276$ °C); however, decomposition still occurred in one step. The reason for the reduced thermal stability of the macroinitiator is the presence of bromoalkyl units, which lead to the removal of HBr upon heating in the TGA analysis

Fig. 3 **a** Monomer consumption vs. reaction time **b** Variation in (Đ) and Mn of PMMA side chains (obtained via hydrolysis of PMMA-*g*-HPC) versus monomer conversion **c** GPC traces of PMMA side chains withdrawn from the reaction mixture at various time intervals

was hydrolyzed to obtain PMMA side chains, GPC traces of PMMA side chains withdrawn from the reaction mixture at various time intervals is given in Fig. 3c. Moreover, during the polymerization process, the Đ reduced while the average molecular weight (Mn) of PMMA increased with increase in monomer conversion, as shown in Table 1. In conclusion, the ATRP was a well-controlled process and these results are consistent with previous studies (Chun-Xiang et al. 2009; Singh et al. 2018).

Thermogravimetric analysis

Thermogravimetric analysis (TGA) was performed to investigate the thermal characteristics of the synthesized polymers. It was previously established that the thermal stability of cellulose and its derivatives is significantly influenced by the substituent groups

Table 2 TGA analysis of macroinitiator, HPC-0, CP-06, CP-08, and CP-12

Samples	T_5 (°C)	T_{10} (°C)	T_{50} (°C)	R_{600} (%)
Macroinitiator	256	265	276	24
HPC-0	330	350	375	31
CP-06	267	277	386	19
CP-08	276	287	403	22
CP-12	290	305	422	23

T_5, T_{10}, and T_{50} denote temperatures at which 5, 10, and 50% weight loss occur. R_{600} is the residual mass at 600 °C

(Oestmark et al. 2007). In case of CP-12, the thermal degradation occurs in two steps, as shown in Fig. 4. The initial small weight loss can be attributed to the removal of trapped moisture at approximately 100 °C. The first degradation step ranged from 281 to 315 °C.
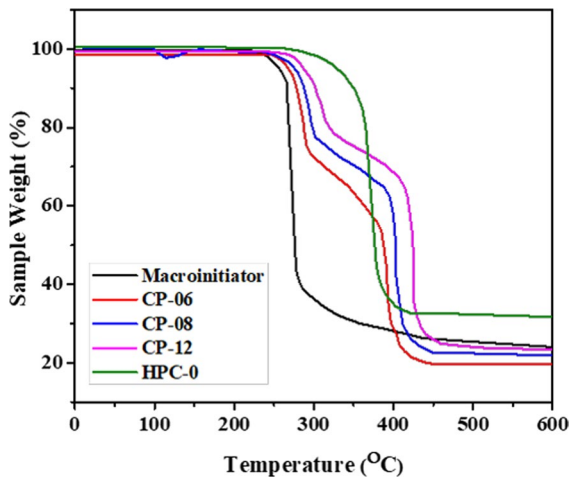
Fig. 4 TGA of macroinitiator, CP-06, CP-08, CP-12 and HPC-0

The second degradation step started at approximately 400 °C and continued until 470 °C. In CP-12, the value of T_{50} was 422 °C, which is higher than the T_{50} values of HPC-0 and the macroinitiator due to chain extension in the final polymer. Similarly, CP-12 exhibited a lower R_{600} value than HPC-0 and the macroinitiator did. The thermal stabilities of CP-06 and CP-08 demonstrate a similar trend to that of CP-12, as shown in Fig. 4; Table 2. From these data, it can be concluded that the thermal stability of the polymers was quite different from that of HPC-0 and the macroinitiator, which in turn confirmed the successful synthesis of the polymers.

The thermoresponsive behaviors of the polymers

The thermoresponsive behaviors of HPC-0, CP-06, CP-08, and CP-12 in aqueous solutions were investigated. The transmittance of the CP-12 aqueous solution as a function of the temperature at different pH values and the LCST as a function of the pH are shown in Fig. 5a, b respectively. As obvious from the Fig. 5a, the LCST of CP-12 moved to a lower temperature as the pH of the solutions increased. Furthermore, the transmittance of the polymer solutions decreased to approximately 80% and 75% at low pH values of 3.5 and 5.0, respectively, as shown in Fig. 5a. This can be attributed to some fraction of self-assembled polymer chains (Ma et al. 2010a, b). It is well established that, in an acidic

aqueous solution, PMMA chains of PMMA-*g*-HPC can be protonated, which can enhance the electrostatic forces of repulsion, which in turn can inhibit phase separation(Mahltig et al. 2003). Similarly, it is obvious from Fig. 5b that grafting of PMMA chains on HPC decreased the LCST from 44.3 to 36.7 °C when the pH was increased from 3.5 to 12.1. This is consistent with previously published literature (Zhang et al. 2021). To evaluate these properties, the thermoresponsive behavior of HPC-0, as a function of temperature at different pH values, was also investigated, as shown in Fig. 5c. While Fig. 5d exhibits the dependence of LCST on pH values for HPC-0. The obtained results revealed that a decrease in pH shifted the LCST of HPC-0 to a lower temperature, which can be attributed to the formation of hydrophobic aggregates originating from the disruption of hydrogen bonds between water molecules and HPC (Bai et al. 2022; Bonetti et al. 2021). The decreased LCST of CP-12 compared to that of HPC-0 is associated with hydrogen bond formation between the hydrogen bond donor (HPC) and ester groups of PMMA (hydrogen bond acceptor). It can be inferred that CP-12 exhibited LCST behavior at approximately 36.7 °C that falls in the physiological temperature range (25–38 °C), making it suitable for in vivo drug delivery systems.

In the case of CP-06 and CP-08, similar effects were observed, i.e., by increasing the pH, the LCST of the polymer decreased. It was found that at pH-12.1, LCST was 42.3 °C and 39.8 °C for CP-06 and CP-08, respectively, as shown in Fig. 6. Overall, the different LCST trend between the HPC and PMMA-*g*-HPC series depending on pH was summarized in Scheme 2. The LCST of HPC in basic solution is relatively higher than LCST in acidic solution, whereas the LCST of PMMA-*g*-HPC is relatively higher in acidic rather than in basic solution. The effect is further illustrated in Scheme 2b, at a temperature below the LCST, PMMA-g-HPC is soluble in the solvent. The polymer chains are hydrated and interact with the solvent molecules, maintaining a homogeneous solution. This is because the hydroxypropyl cellulose component forms hydrogen bonds with the solvent, promoting solvation. As the temperature exceeds the LCST, the polymer-solvent interactions weaken, and the balance between the polymer-solvent and polymer-polymer interactions shifts. This results in the
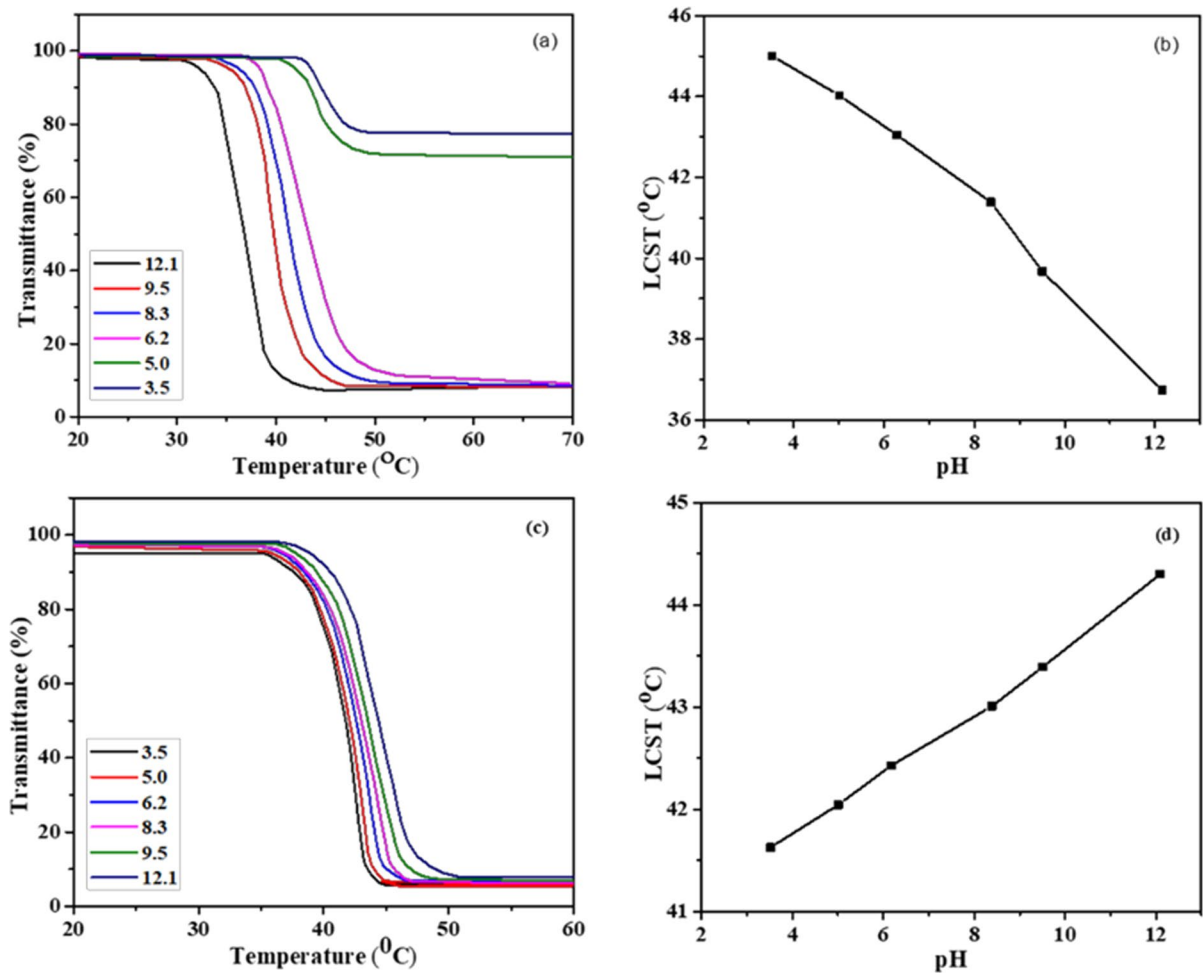
Fig. 5 **a**, **c** Transmittance of CP-12 and HPC-0 as a function of temperature (20–70 °C) at different pH values, respectively. **b**, **d** The LCST of CP-12 and HPC-0 as a function of pH values

aggregation or phase separation of PMMA-g-HPC. The lower LCST of PMMA-*g*-HPC as compare to HPC can be explained on the bases of dominant hydrophobic behavior of polymer when PMMA was grafted on HPC. The grafted PMMA chains also acted as spacers and pushed HPC chains apart from each other, which further decreased the hydrophilic interactions. These findings are in good agreement with previously published literature (Shao et al. 2011).

Figure 7 shows the optical density of HPC-0, CP-06, CP-08 and CP-12 measured at 550 nm by heating the solutions from 20 to 70 °C. HPC-0 has a negligible optical density (0.095 from 20 to 44.3 °C), which shows the high solubility of

HPC-0 in water within this temperature range. However, when the temperature was raised from 44.3 to 70 °C, HPC-0 became insoluble, and its optical density was enhanced to 1.17. The temperature after which the polymer becomes hydrophobic and insoluble in water is termed its LCST point; therefore, the LCST of HPC-0 is 44.3 °C (Chiang 2016). The insolubility of all polymers above their LCST was due to the phase transition phenomenon that resulted in the formation of precipitates. This is in good agreement with previous literature (Chiang 2016). While CP-06 displayed an optical density of 0.097, which remained constant till 42.3 °C and then increased to 1.50 at 70 °C, which indicates that the solution heated above 42.3 °C makes
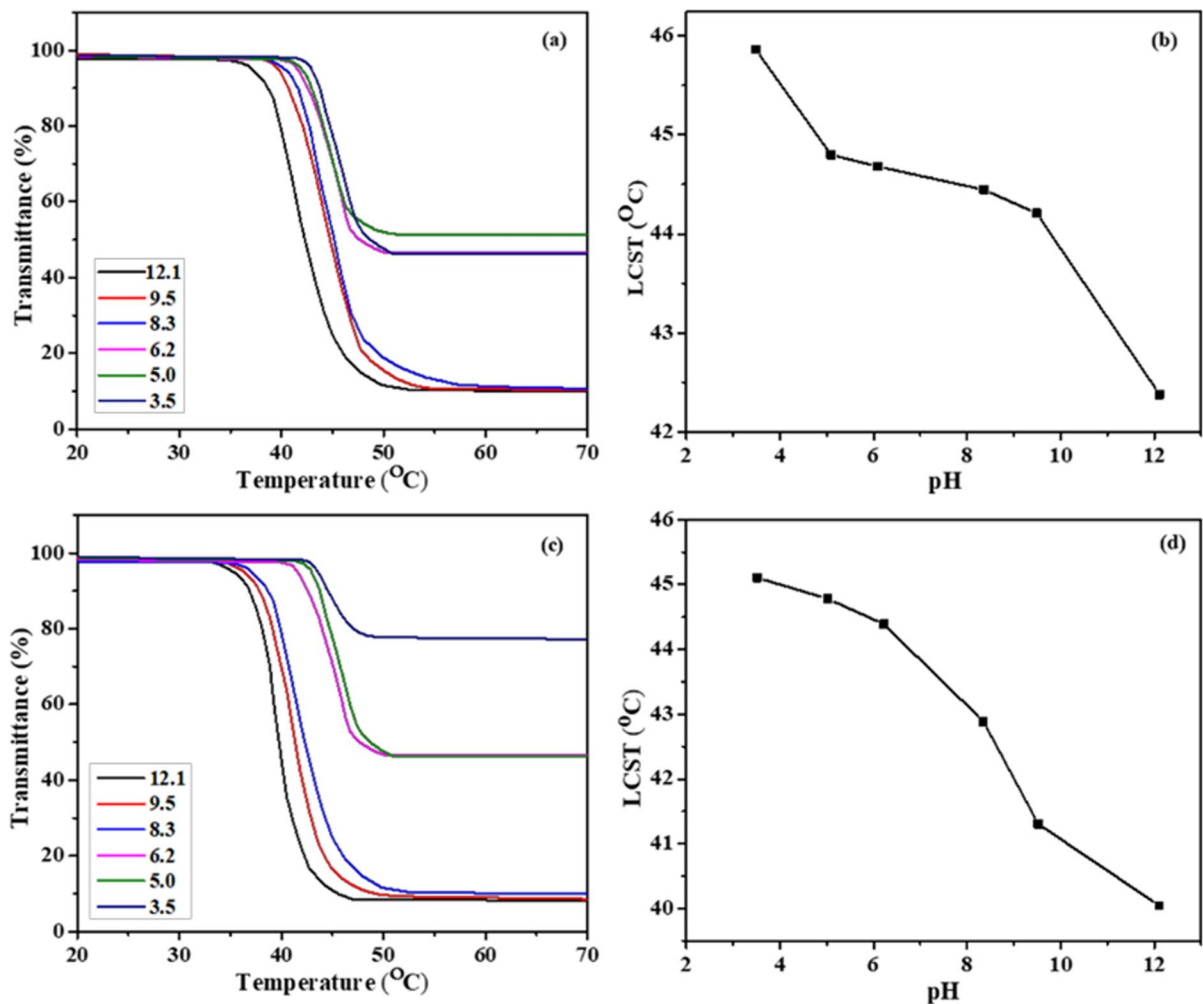
Fig. 6 **a**, **c** Transmittance of CP-06 and CP-08 as a function of temperature (20–70 °C) at different pH values, respectively. **b**, **d** The LCST of CP-06 and CP-08 as a function of pH values

the polymer insoluble in an aqueous solution. Similarly, CP-08 showed an optical density of 1.58 at 70 °C, while its value remained almost constant at 0.097 from 20 to 39.8 °C. Likewise, CP-12 exhibited an optical density of 0.098 from 20 to 36.7 °C and then its value increased as the temperature increased from 36.7 to 70 °C. At 70 °C, it had a value of 1.72. This increase in the optical density at higher temperatures can be attributed to the dehydration of the hydroxypropyl cellulose units, resulting in increased hydrophobic interactions among the PMMA segments (Wei et al. 2006). It is well reported that the incorporation of hydrophobic segments in the polymer backbone results in a

decrease in the LCST (Park et al. 2022). Thus, in CP-06, CP-08, and CP-12, the hydrophobic PMMA segments are increased compared to HPC-0, resulting in an increased optical density and a decrease in the LCST value. Therefore, these temperature-driven changes in the optical density of the polymeric solutions are related to the increase in the hydrophobic PMMA segments. In addition, as evident from the above data, the optical density and thermoresponsive behavior of all the polymers complement each other.

Moreover, a comparative study of synthesis of thermoresponsive polymers in our study and
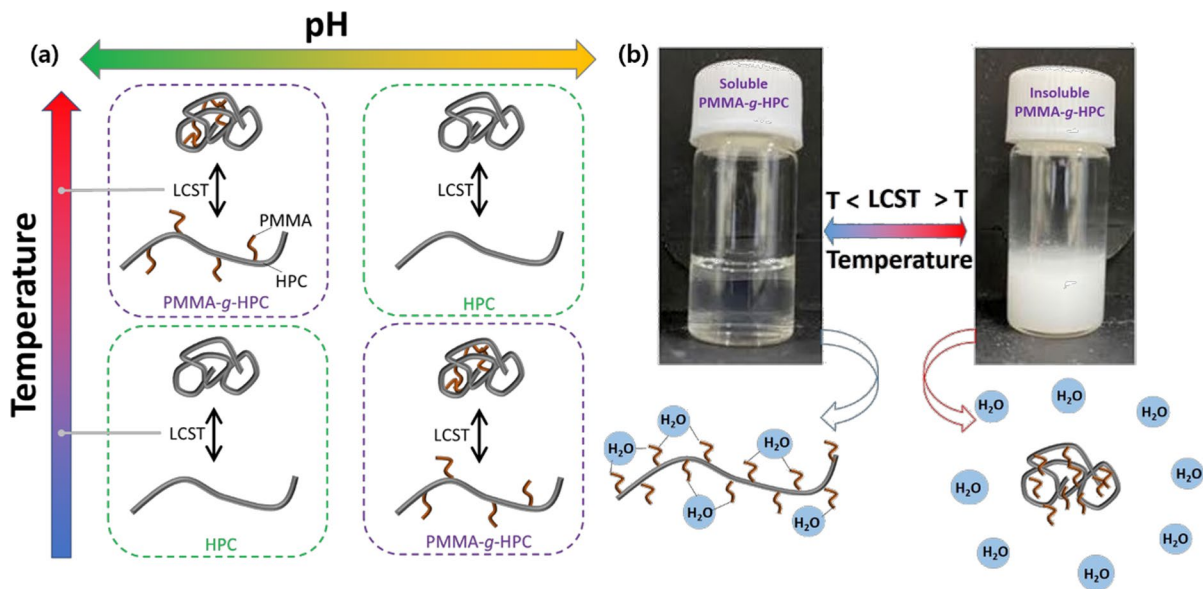
Scheme 2 a Illustration of pH dependent LCST difference between HPC and PMMA-*g*-HPC, **b** Mechanism of thermoresponsive behavior of the PMMA-*g*-HPC.

the previously published literature is given in the Table 3.

Conclusion

To summarize, under visible-light irradiation and with 4CzIPN serving as the photoredox catalyst, metal-free PMMA-*g*-HPC with a narrow Đ was successfully synthesized through O-ATRP. In this approach, HPC was first converted into a macroinitiator by reacting with 2-bromopropionyl bromide. Then, this macroinitiator was utilized for grafting PMMA chains on HPC via O-ATRP, leading to the synthesis of thermoresponsive polymers, which were thoroughly characterized by FTIR, NMR, TGA, and GPC. The thermo-responsive properties of these polymers in aqueous solutions were investigated by measuring the LCST of the polymers as a function of temperature at different pH values. The LCST of PMMA-*g*-HPC decreased from 44.3 to 36.7 °C, when the pH increased from 3.5 to 12.1 in the case of CP-12, which has the highest MW for grafting PMMA, whereas pristine HPC increases its LCST from 41.6 to 44.3 °C with increasing pH value from 3.5 to 12.1. The MW of grafted PMMA influenced
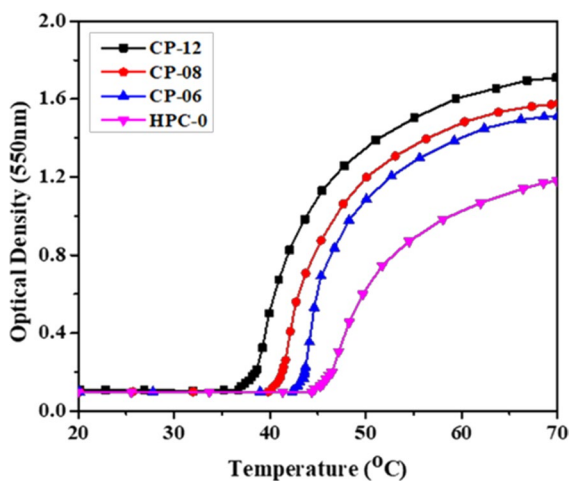
Fig. 7 Optical density of HPC-0, CP-06, CP-08, and CP-12 polymers in an aqueous solution

the trend and degree of pH dependency of the LCST of HPC derivatives. We anticipate that the synthesized metal-free, thermo-responsive polymer in a wide pH range is promising for a range of biological, electrical, and biosensor applications, especially in drug delivery systems.

Table 3 A comparison of our data with the previously prepared cellulose based grafted polymers

Sr. No	Polymer	Mn	Đ	LCST (°C)	References
1	HPC-g-P(NIPAAm)	4.06×10^4–7.18×10^4	1.8–1.9	33.3–34.7	Xu et al. (2010)
2	PMMA-g-PTh	22,864	1.68	LCST was not measured	Massoumi and Jaymand (2016)
3	PMMA-PFPMA,	22,100–36,100	1.45–1.98	LCST was not measured	Zhang et al. (2012)
4	PMMA-b-PNIPAM	41,000	1.3	LCST was not measured	Ko et al. (2020)
5	BiB-CNCs	5300–46,500	1.07–1.10	LCST was not measured	Hatton et al. (2017)
6	PDMAEMA	2500–8600	1.1–1.2	LCST was not measured	Arredondo et al. (2020)
7	HPC-g-PMMA	291,075	1.1	36.7	This work

Data availability Not applicable.

Declarations

Conflict of interest The authors declare no conflict of interest.

Ethics approval and consent to participate The manuscript does not contain any unethical data, tables, images, or reports. No data, table, or figure has been copied from another source. Also, after publishing this paper, there won't be any ethical problems.

Consent for publication Not applicable.

References

Arredondo J, Woodcock NM, Garcia-Valdez O, Jessop PG, Champagne P, Cunningham MF (2020) Surface modification of cellulose nanocrystals via RAFT polymerization of CO_2-responsive monomer-tuning hydrophobicity. Langmuir 36:13989–13997

Bagheri M, Pourmirzaei L (2013) Synthesis and characterization of cholesteryl-modified graft copolymer from hydroxypropyl cellulose and its application as nanocarrier. Macromol Res 21:801–808

Bai Y, Zhang Z, Zhang A, Chen L, He C, Zhuang X, Chen X (2012) Novel thermo-and pH-responsive hydroxypropyl cellulose-and poly(l-glutamic acid)-based microgels for oral insulin controlled release. Carbohydr Polym 89:1207–1214

Bai Y, Chen W, Tang T, He Y (2022) Photothermal enhancement of reduced graphene oxide in hydroxypropyl cellulose for a smart-window application. Sol Energy 245:376–384

Barty-King CH, Chan CLC, Parker RM, Bay MM, Vadrucci R, De Volder M, Vignolini S (2021) Mechanochromic, structurally colored, and edible hydrogels prepared from hydroxypropyl cellulose and gelatin. Adv Mater 33:2102112

Bonetti L, De Nardo L, Farè S (2021) Thermo-responsive methylcellulose hydrogels: from design to applications as smart biomaterials. Tissue Eng Part B Rev 27:486–513

Chang C, Wei H, Wu D-Q, Yang B, Chen N, Cheng S-X, Zhang X-Z, Zhuo R-X (2011) Thermo-responsive shell cross-linked PMMA-bP (NIPAAm-co-NAS) micelles for drug delivery. Int J Pharm 420:333–340

Chen M, Zhong M, Johnson JA (2016) Light-controlled radical polymerization: mechanisms, methods, and applications. Chem Rev 116:10167–10211

Chiang FB (2016) Temperature-responsive hydroxypropylcellulose based thermochromic material and its smart window application. RSC Adv 6:61449–61453

Chun-xiang L, Huai-yu Z, Ming-hua L, Shi-yu F, Jia-jun Z (2009) Preparation of cellulose graft poly(methyl methacrylate) copolymers by atom transfer radical polymerization in an ionic liquid. Carbohydr Polym 78:432–438

Ci J, Kang H, Liu C, He A, Liu R (2017) Thermal sensitivity and protein anti-adsorption of hydroxypropyl cellulose-g-poly(2-(methacryloyloxy) ethyl phosphorylcholine). Carbohydr Polym 157:757–765

Cobo I, Li M, Sumerlin BS, Perrier S (2015) Smart hybrid materials by conjugation of responsive polymers to biomacromolecules. Nat Mater 14:143–159

de Ávila Gonçalves S, Rodrigues R, Pioli Vieira P (2021) Metal-free organocatalyzed atom transfer radical polymerization: synthesis, applications, and future perspectives. Macromol Rapid Commun 42:2100221

Discekici EH, Anastasaki A, Kaminker R, Willenbacher J, Truong NP, Fleischmann C, Oschmann B, Lunn DJ, Read de Alaniz J, Davis TP (2017) Light-mediated atom transfer radical polymerization of semi-fluorinated (meth)

acrylates: facile access to functional materials. J Am Chem Soc 139:5939–5945

Droguet BE, Liang H-L, Frka-Petesic B, Parker RM, De Volder MF, Baumberg JJ, Vignolini S (2022) Large-scale fabrication of structurally coloured cellulose nanocrystal films and effect pigments. Nat Mater 21:352–358

Dupayage L, Nouvel C, Six J-L (2011) Protected versus unprotected dextran macroinitiators for ATRP synthesis of Dex-g-PMMA. J Polym Sci Part A Polym Chem 49:35–46. https://doi.org/10.1002/pola.24409

Garcia-Valdez O, Champagne P, Cunningham MF (2018) Graft modification of natural polysaccharides via reversible deactivation radical polymerization. Prog Polym Sci 76:151–173

Hatton FL, Kedzior SA, Cranston ED, Carlmark A (2017) Grafting-from cellulose nanocrystals via photoinduced Cu-mediated reversible-deactivation radical polymerization. Carbohydr Polym 157:1033–1040

Huang C-F, Chen J-K, Tsai T-Y, Hsieh Y-A, Andrew Lin K-Y (2015) Dual-functionalized cellulose nanofibrils prepared through TEMPO-mediated oxidation and surface-initiated ATRP. Polymer 72:395–405. https://doi.org/10.1016/j.polymer.2015.02.056

Jana S, Uchman M (2020) Poly(2-oxazoline)-based stimulus-responsive (Co)polymers: an overview of their design, solution properties, surface-chemistries and applications. Prog Polym Sci 106:101252

Jia H, Teng Y, Li N, Li D, Dong Y, Zhang D, Liu Z, Zhao D, Guo X, Di W (2022) Dual stimuli-responsive inks based on orthogonal upconversion three-primary-color luminescence for advanced anticounterfeiting applications. ACS Mater Lett 4:1306–1313

Jin X, Kang H, Liu R, Huang Y (2013) Regulation of the thermal sensitivity of hydroxypropyl cellulose by poly(N-isopropylacryamide) side chains. Carbohydr Polym 95:155–160

Kaldéus T, Telaretti Leggieri MR, Cobo Sanchez C, Malmström E (2019) All-aqueous SI-ARGET ATRP from cellulose nanofibrils using hydrophilic and hydrophobic monomers. Biomacromolecules 20:1937–1943

Kang H, Liu R, Huang Y (2013) Cellulose derivatives and graft copolymers as blocks for functional materials. Polym Int 62:338–344

Kasaai MR (2008) Calculation of viscometric constants, hydrodynamic volume, polymer–solvent interaction parameter, and expansion factor for three polysaccharides with different chain conformations. Carbohydr Res 343:2266–2277

Kedzior SA, Zoppe JO, Berry RM, Cranston ED (2019) Recent advances and an industrial perspective of cellulose nanocrystal functionalization through polymer grafting. Curr Opin Solid State Mater Sci 23:74–91

Ko C-H, Henschel C, Meledam GP, Schroer MA, Müller-Buschbaum P, Laschewsky A, Papadakis CM (2020) Self-assembled micelles from thermoresponsive poly(methyl methacrylate)-b-poly(N-isopropylacrylamide) diblock copolymers in aqueous solution. Macromolecules 54:384–397

Lacerda PSS, Barros-Timmons AMMV, Freire CSR, Silvestre AJD, Neto CP (2013) Nanostructured composites obtained by ATRP sleeving of bacterial cellulose

nanofibers with acrylate polymers. Biomacromolecules 14:2063–2073. https://doi.org/10.1021/bm400432b

Larsson E, Pendergraph SA, Kaldéus T, Malmström E, Carlmark A (2015) Cellulose grafting by photoinduced controlled radical polymerisation. Polym Chem 6:1865–1874

Ma L, Kang H, Liu R, Huang Y (2010) Smart assembly behaviors of hydroxypropylcellulose-graft-poly(4-vinyl pyridine) copolymers in aqueous solution by thermo and pH stimuli. Langmuir 26:18519–18525

Ma L, Liu R, Tan J, Wang D, Jin X, Kang H, Wu M, Huang Y (2010) Self-assembly and dual-stimuli sensitivities of hydroxypropylcellulose-graft-poly(N, N-dimethyl aminoethyl methacrylate) copolymers in aqueous solution. Langmuir 26:8697–8703

Mahltig B, Jérôme R, Stamm M (2003) The influence of an acid–base-equilibrium on the adsorption behaviour of a weak polyampholyte. J Polym Res 10:219–223

Massoumi B, Jaymand M (2016) Chemical and electrochemical grafting of polythiophene onto poly(methyl methacrylate), and its electrospun nanofibers with gelatin. J Mater Sci: Mater Electron 27:12803–12812

Matyjaszewski K (2018) Advanced materials by atom transfer radical polymerization. Adv Mater 30:1706441

Matyjaszewski K, Tsarevsky NV (2014) Macromolecular engineering by atom transfer radical polymerization. J Am Chem Soc 136:6513–6533

Miyake GM, Theriot JC (2014) Perylene as an organic photocatalyst for the radical polymerization of functionalized vinyl monomers through oxidative quenching with alkyl bromides and visible light. Macromolecules 47:8255–8261

Morandi G, Heath L, Thielemans W (2009) Cellulose nanocrystals grafted with polystyrene chains through surface-initiated atom transfer radical polymerization (SI-ATRP). Langmuir 25:8280–8286. https://doi.org/10.1021/la900452a

Nada A, Hassan ML (2000) Thermal behavior of cellulose and some cellulose derivatives. Polym Degrad Stab 67:111–115

Oestmark E, Harrisson S, Wooley KL, Malmström EE (2007) Comb polymers prepared by ATRP from hydroxypropyl cellulose. Biomacromolecules 8:1138–1148

Pan X, Fang C, Fantin M, Malhotra N, So WY, Peteanu LA, Isse AA, Gennaro A, Liu P, Matyjaszewski K (2016) Mechanism of photoinduced metal-free atom transfer radical polymerization: experimental and computational studies. J Am Chem Soc 138:2411–2425

Park CH, Lee S, Pornnoppadol G, Nam YS, Kim S-H, Kim BJ (2018) Microcapsules containing pH-responsive, fluorescent polymer-integrated MoS$_2$: an effective platform for in situ pH sensing and photothermal heating. ACS Appl Mater Interfaces 10:9023–9031

Park SC, Sharma G, Kim J-C (2022) Synthesis of temperature-responsive P(vinyl pyrrolidone-co-methyl methacrylate) micelle for controlled drug release. J Dispers Sci Technol 43:461–470

Parkatzidis K, Wang HS, Truong NP, Anastasaki A (2020) Recent developments and future challenges in controlled radical polymerization: a 2020 update. Chem 6:1575–1588

Porsch C, Hansson S, Nordgren N, Malmström E (2011) Thermo-responsive cellulose-based architectures: tailoring LCST using poly(ethylene glycol) methacrylates. Polym Chem 2:1114–1123

Rahimian K, Wen Y, Oh JK (2015) Redox-responsive cellulose-based thermoresponsive grafted copolymers and insitu disulfide crosslinked nanogels. Polymer 72:387–394

Rwei S-P, Nguyen T-A (2015) Formation of liquid crystals and behavior of LCST upon addition of xanthan gum (XG) to hydroxypropyl cellulose (HPC) solutions. Cellulose 22:53–61

Saad A, Mills R, Wan H, Ormsbee L, Bhattacharyya D (2020) Thermoresponsive PNIPAm–PMMA-functionalized PVDF membranes with reactive Fe–Pd nanoparticles for PCB degradation. Ind Eng Chem Res 59:16614–16625

Shao P, Wang B, Wang Y, Li J, Zhang Y (2011) The application of thermosensitive nanocarriers in controlled drug delivery. J Nanomater 2011:1–12

Sikdar P, Uddin MM, Dip TM, Islam S, Hoque MS, Dhar AK, Wu S (2021) Recent advances in the synthesis of smart hydrogels. Mater Adv 2:4532–4573

Singh VK, Yu C, Badgujar S, Kim Y, Kwon Y, Kim D, Lee J, Akhter T, Thangavel G, Park LS (2018) Highly efficient organic photocatalysts discovered via a computer-aided-design strategy for visible-light-driven atom transfer radical polymerization. Nat Catal 1:794–804

Theriot JC, Lim C-H, Yang H, Ryan MD, Musgrave CB, Miyake GM (2016) Organocatalyzed atom transfer radical polymerization driven by visible light. Science 352:1082–1086

Treat NJ, Sprafke H, Kramer JW, Clark PG, Barton BE, Read de Alaniz J, Fors BP, Hawker CJ (2014) Metal-free atom transfer radical polymerization. J Am Chem Soc 136:16096–16101

Tu C-W, Tsai F-C, Chang C-J, Yang C-H, Kuo S-W, Zhang J, Chen T, Huang C-F (2019) Surface-initiated initiators for continuous activator regeneration (SI ICAR) ATRP of MMA from 2,2,6,6–tetramethylpiperidine–1–oxy (TEMPO) oxidized cellulose nanofibers for the preparations of PMMA nanocomposites. Polymers 11:1631

Wei H, Zhang X-Z, Zhou Y, Cheng S-X, Zhuo R-X (2006) Self-assembled thermoresponsive micelles of poly(N-isopropylacrylamide-b-methyl methacrylate). Biomaterials 27:2028–2034

Weißenborn E, Braunschweig B (2019) Hydroxypropyl cellulose as a green polymer for thermo-responsive aqueous foams. Soft Matter 15:2876–2883

Wohlhauser S, Delepierre G, Labet M, Gl Morandi, Thielemans W, Weder C, Zoppe JO (2018) Grafting polymers from cellulose nanocrystals: synthesis, properties, and applications. Macromolecules 51:6157–6189

Xu F, Zhu Y, Liu F, Nie J, Ma J, Yang W (2010) Comb-shaped conjugates comprising hydroxypropyl cellulose backbones and low-molecular-weight poly(N-isopropylacryamide) side chains for smart hydrogels: synthesis, characterization, and biomedical applications. Bioconjug Chem 21:456–464

Yi J, Xu Q, Zhang X, Zhang H (2008) Chiral-nematic self-ordering of rodlike cellulose nanocrystals grafted with poly(styrene) in both thermotropic and lyotropic states. Polymer 49:4406–4412. https://doi.org/10.1016/j.polymer.2008.08.008

Yuan W, Zhang J, Zou H, Shen T, Ren J (2012) Amphiphilic ethyl cellulose brush polymers with mono and dual side chains: facile synthesis, self-assembly, and tunable temperature-pH responsivities. Polymer 53:956–966

Zhang Q, Schattling P, Theato P, Hoogenboom R (2012) Tuning the upper critical solution temperature behavior of poly(methyl methacrylate) in aqueous ethanol by modification of an activated ester comonomer. Polym Chem 3:1418–1426

Zhang X, Zhang J, Dong L, Ren S, Wu Q, Lei T (2017) Thermoresponsive poly(poly(ethylene glycol) methylacrylate) s grafted cellulose nanocrystals through SI-ATRP polymerization. Cellulose 24:4189–4203

Zhang L, Xia H, Xia F, Du Y, Wu Y, Gao Y (2021) Energy-saving smart windows with HPC/PAA hybrid hydrogels as thermochromic materials. ACS Appl Energy Mater 4:9783–9791